**Wind and Structures**, *Vol. 23, No. 3 (2016) 253-273*
DOI: http://dx.doi.org/10.12989/was.2016.23.3.253 

# Aerodynamic stability of iced stay cables on cable-stayed bridge

Shouying Li*[1], Teng Wu[2], Tao Huang[1] and Zhengqing Chen[1]

[1]*Key Laboratory for Wind and Bridge Engineering of Hunan Province, College of Civil Engineering, Hunan University, Changsha 410082, China*
[2]*Department of Civil, Structural and Environmental Engineering, University at Buffalo-The State Univ. of New York, Buffalo, NY 14260, USA*

*(Received April 21, 2015, Revised June 15, 2016, Accepted June 30, 2016)*

**Abstract.** Ice accretions on stay cables may result in the instable vibration of galloping, which would affect the safety of cable-stayed bridges. A large number of studies have investigated the galloping vibrations of transmission lines. However, the obtained aerodynamics in transmission lines cannot be directly applied to the stay cables on cable-stayed bridges. In this study, linear and nonlinear single degree-of-freedom models were introduced to obtain the critical galloping wind velocity of iced stay cables where the aerodynamic lift and drag coefficients were identified in the wind tunnel tests. Specifically, six ice shapes were discussed using section models with geometric scale 1:1. The results presented obvious sudden decrease regions of the aerodynamic lift coefficient for all six test models. Numerical analyses of iced stay cables associated to a medium-span cable-stayed bridge were carried out to evaluate the potential galloping instability. The obtained nonlinear critical wind velocity for a 243-meter-long stay cable is much lower than the design wind velocity. The calculated linear critical wind velocity is even lower. In addition, numerical analyses demonstrated that increasing structural damping could effectively mitigate the galloping vibrations of iced stay cables.

**Keywords:** galloping vibrations; stay cables; ice accretions; aerodynamic force coefficients; critical wind velocity

## 1. Introduction

Stay cables of cable-stayed bridges, due to its light mass, low natural frequency and small structural damping, may experience several types of wind-induced vibrations, such as rain-wind induced vibration(Hikami and Shiraishi 1988, Li *et al*. 2013), vortex induced vibration (Zuo *et al*. 2008, 2001), and buffeting (Jones *et al*. 1997). However, it is well known that stay cables of cable-stayed bridges are free of galloping vibrations since they possess a circular cross section. In the case that there is a yaw angle (wind direction is not perpendicular to the cable longitudinal axis), the effective cross section of stay cables become an ellipse shape, and the so-called dry galloping may occur (Flamand and Boujard 2009, Cheng *et al*. 2008a). Macdonald and Larose (2008a, 2008b) proposed a two degrees-of-freedom (DOFs) theoretical model for simulating dry galloping, where the quasi-steady assumption was adopted. Besides dry galloping, stay cables may

*Corresponding author, Associate Professor, E-mail: shyli@hun.edu.cn


http://www.techno-press.org/?journal=was&subpage=8 ISSN: 1226-6116 (Print), 1598-6225 (Online)

experience galloping vibration if some small components (or surface protrusion) are attached on the cable surface. Li *et al*. (2014) investigated the aerodynamic effects of lamp installation on the stay cables of Hedong cable-stay Bridge in China based on the wind tunnel tests and CFD simulations. It is found that galloping vibration appeared at the wind velocity around 18 m/s.

Another common small surface protrusion for structures is the ice accretion resulting from special atmospheric environment, e.g., hoar frost, in-cloud icing and precipitation icing (Farzaneh 2008). The effects of ice accretion have been investigated in the areas of power transmission lines (Farzaneh 2008), aviation (Lynch and Khodadoust 2001), and wind energy (Makkonen *et al*. 2001). In fact, galloping vibration was firstly observed on power transmission lines attached with ice accretion. Den Hartog (1956) treated galloping as a velocity-dependent, damping-controlled instability. To investigate its mechanism, Den Hartog (1956) studied the galloping by using a single degree-of-freedom (DOF) linear oscillator, where the linear critical wind velocity of galloping could be obtained. Parkinson and Smith (1964) conducted nonlinear analyses to estimate the amplitude and frequency of galloping by means of the so-called Krylov-Bogoliubov method. While it is straightforward to utilize the classical linear and nonlinear galloping theories to simulate the aerodynamics of iced stay cables, it is extremely difficult to determine the exact shape of ice accretion. Few public reports concerning field observations of ice shapes are available. Experimental simulations for ice shapes, e.g., in-cloud icing (Laforte *et al*. 1984, Kollár and Farzaneh 2010) and freezing rain (Stumpf 1994, Lu *et al*. 2000), seem to be a more feasible way to study the ice shape. In addition, theoretical icing models could be established to predict ice shape (Poots 1996, Farzaneh 2008, Fu *et al*. 2006), however, usually there is a large discrepancy between the prediction and experimental results. The Electric Power Research Institute in USA has suggested several ice shapes for transmission lines, including the crescent-shape and D-shape (Alto 1979).

Full-scale experiments carried out by Koss *et al*. (2013) indicated that ice accretion could be produced on the bridge cable under the environment of light precipitation at moderate low temperatures (from 0º to 5º). Large oscillations of iced stay cables will significantly shorten its fatigue life, and more importantly, result in falling ice that becomes a safety issue for motorists and pedestrians (Gimsing and Georgakis 2012). Recently, a series of wind tunnel tests were carried out in the special climatic wind tunnel to investigate the ice shape on bridge cables. Koss *et al*. (2012) studied the ice shape on vertical and horizontal cables. It is found that the ice shape achieved at low temperature is like D-shape, and crescent-shape at high temperature. Demartino *et al*. (2015) extended their study on the ice shape of inclined stay cable, and measured the aerodynamic forces on the bridge cables attached with ice accretion. The results of Koss *et al*. (2012) and Demartino *et al*. (2015) both indicated that there is no a single cross section that can fully represent all the key features of ice shape on stay cables.

By using artificial ice accretion of crescent-shape, Gjelstrup *et al*. (2012) conducted static and dynamic wind tunnel tests to measure the aerodynamic forces and oscillation responses of a segmental model. Theoretical analysis method was also adopted to investigate the galloping instability of stay cables attached with ice accretion in recent years. Gjelstrup and Georgakis (2011) proposed a three DOFs theoretical model based on quasi-steady assumption to determine the onset of ice accretion induced galloping. Demartino and Ricciardelli (2015) compared several quasi-steady theory based models for the galloping instability of stay cables with ice accretion, where dependency of the aerodynamic coefficients on the angle of attack, wind-cable angle and Reynolds number is discussed.

However, little attention was paid to the critical wind velocity of real stay cables on cable

stayed bridges. Compared with transmission lines, stay cables have a larger diameter, higher axial tension and natural frequency, and a heavier mass per unit length. These structural properties may play a significant role in the consideration of oscillation amplitude and critical wind velocity of galloping for iced stay cables. In addition, the effects of mean wind profile within the atmospheric boundary layer cannot be ignored. In this study, the galloping vibration of iced stay cables on a medium-span cable-stayed bridge was comprehensively investigated. First, a series of wind tunnel tests were carried out to obtain the aerodynamic drag and lift coefficients of stay cables attached with various artificial ice accretions. Then, both linear and nonlinear single DOF approaches to calculate the critical wind velocity of stay cables with ice accretions were introduced. Numerical analyses were conducted to obtain the critical wind velocity and galloping vibration amplitude of iced stay cables of the investigated medium-span stay-cable bridge. The obtained results contribute to the bridge design as an important input. Several vibration characteristics such as the time history of vibration amplitude are discussed. Finally, the effects of axial distribution of ice accretion and structural damping on galloping vibration of iced stay cables were analyzed.

## 2. Wind tunnel test set-up

Wind tunnel tests were carried out in the 3 m in width by 2.5 m in height by 17 m in length closed-circuit test section of the HD-2 Boundary Layer Wind Tunnel (HD-2BLWT) in Wind Engineering Research Center, Hunan University, China. The maximum wind velocity of this test section is 58 m/s. HD-2BLWT is a hybrid wind tunnel with two horizontal closed-circuit test sections and one open-circuit test section. The other closed-circuit test section is 5.5 m in width by 4.4 m in height by 15 m in length with a maximum wind velocity of 15 m/s, and the open-circuit test section is 8.2 m in width by 2 m in height by 15 m in length with a maximum wind velocity of 18 m/s.

The diameter and length of the cable model are 120 mm and 600 mm, respectively. The geometric scale of the test models is selected to be 1:1 to eliminate the Reynolds number effects. Two types of ice accretions, namely crescent-shape and D-shape are investigated. More specifically, three shapes are selected for each of them, as shown in Fig. 1. The maximum thicknesses of C1, C2 and C3 are respectively 10, 50 and 80 mm, corresponding to eccentricities of 0.08, 0.42 and 0.66. The maximum thicknesses of D1, D2 and D3 are respectively 30, 55 and 50 mm, corresponding to eccentricities of 0.25, 0.46 and 0.42. A typical photo of the test models is shown in Fig. 2.

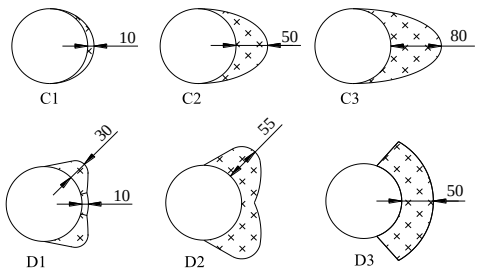


Fig. 1 Ice shapes adopted in the wind tunnel tests (unit: mm)

Fig. 2 Photo of the test models

The test models are made of foam plastic enclosed by balsa, which leads to a very light mass of test model about 0.2 kg and a rather high frequency of test model system around 50 Hz. Relatively high natural frequency of test models compared to that of wind-induced loading is very important in the application of force measurement system since the inertial force resulting from the oscillation of test models during the wind action could be easily removed. A circular end plate with a diameter of 300 mm and a thickness of 10 mm is fixed at the top of the wind tunnel via a steel bar to reduce the end effects. There is a gap of around 5 mm between the end plate and test model. In the wind tunnel tests, it was found that a 5 mm gap between the end plate and test model is enough to ensure the 2-dimensional flow. The test model is installed on the turntable in the test section, and hence the adjustment of wind attack angle is realized by rotating the turntable. The surface friction effects on the oncoming mean wind velocity is within 10% based on the measured results. The sketch of the test model system is shown in Fig. 3(a), and the photo of the test model installed in wind tunnel is given in Fig. 3(b).

Wind tunnel tests were carried out in uniform flow with a velocity of 12 m/s. The definition of wind attack angle is shown in Fig. 4. For the wind attack angle of 0°, the ice accretion locates at the windward side, and the wind direction is parallel to the symmetry axis of the cross sections of the test models. A range of wind attack angles (0~180° with an interval of 2°) were examined. A six-component force balance system was utilized to measure the aerodynamic forces on the iced cable models. The measurement ranges for each component is listed in Table 1, where x and z directions are in the horizontal plane, and y represents the vertical direction.


Fig. 3 The test model system: (a) Sketch of the test model system and (b) Photo of the test model in the wind tunnel

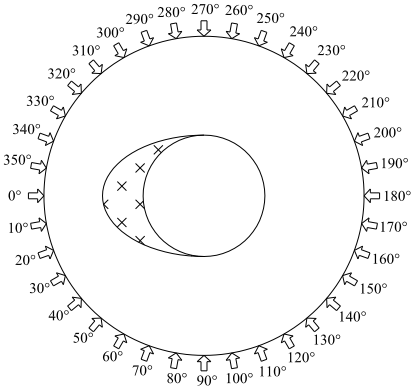


Fig. 4 Definition of wind attack angle

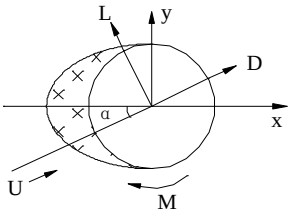


Fig. 5 Body and wind axis coordinate systems

Table 1 Measurement ranges of six-component force balance system

| $y(N)$ | $x(N)$ | $M_z(N\cdot m)$ | $z(N)$ | $M_y(N\cdot m)$ | $M_x(N\cdot m)$ |
|---|---|---|---|---|---|
| 1200 | 300 | 200 | 500 | 100 | 100 |

The aerodynamic forces FX and FY directly obtained from the force balance system are usually referred to the body axis coordinate system oxy, as indicated in Fig. 5. The corresponding aerodynamic force coefficients, CX and CY, can be expressed as

$$C_X = 2F_X / (\rho U^2 LB) \tag{1}$$

$$C_Y = 2F_Y / (\rho U^2 LB) \tag{2}$$

where $\rho$=1.225 kg/m$^3$ is the air density; $U$=12 m/s is the approaching wind velocity; $L$=600 mm is the length of the test model; $B$=120 mm is the diameter of the cable.

The aerodynamic drag and lift coefficients, CD and CL, in the wind axis coordinate system can be calculated using CX and CY as

$$\begin{pmatrix} C_L \\ C_D \end{pmatrix} = \begin{pmatrix} \cos\alpha & -\sin\alpha \\ \sin\alpha & \cos\alpha \end{pmatrix} \begin{pmatrix} C_X \\ C_Y \end{pmatrix} \tag{3}$$

where α is the wind attack angle, as indicated in Fig. 5.

## 3. Results of wind tunnel tests

### 3.1 Aerodynamic drag and lift coefficients

Fig. 6 presents the aerodynamic lift and drag coefficients of the test models with crescent-shape ice accretions (C1, C2 and C3). It could be found from Fig. 6 that the aerodynamic lift coefficients of the test models C1, C2 and C3 all have a sudden decrease around the wind attack angle of 40°, from 0.5 to 0, from 0.8 to 0.2, from 1.0 to 0.4, respectively. The sudden decrease of the aerodynamic lift coefficient implies that the cable with the crescent-shape ice accretions is susceptible to the galloping vibration as the wind attack angle is around 40°. Compared with the test model C1, the aerodynamic lift coefficients of the test model C2 and C3 both have an additional sudden decrease near the wind attack angle of 180°, which means another galloping-prone region. It appears that there are more instable regions of wind attack angle with the increase of the thickness of crescent-shape ice accretion. The aerodynamic drag coefficients of test model C1, C2 and C3 all have their maximum values, around 0.6, 0.8 and 1.0, respectively, near the wind attack angle of 90°. It seems that the windward area of test model has a dominant effect on the aerodynamic drag coefficient. The aerodynamic drag coefficients of the test models in this study are obviously smaller than the classical result, approximately 1.2, of a smooth cylinder within the subcritical region. This could be attributed to the drag crisis at the critical Reynolds number (here in the wind tunnel tests Re=0.9936×105) and the surface roughness of the test models. Generally, the variations of the aerodynamic forces with the wind attack angle have a similar trend for test models C1, C2 and C3.

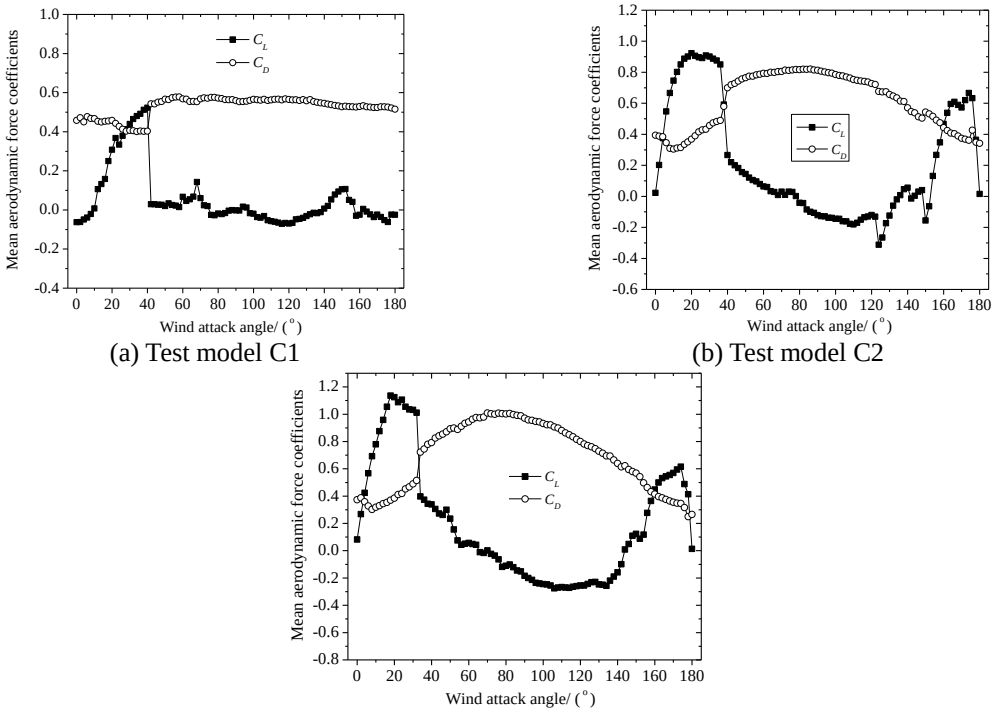


(a) Test model C1 (b) Test model C2

(c) Test model C3

Fig. 6 Aerodynamic drag and lift coefficients for the test models with crescent-shape ice accretions

Fig. 7 shows the aerodynamic lift and drag coefficients of the test models with D-shape ice accretions (D1, D2 and D3). It could be found from Fig. 7 that the variations of the drag and lift coefficients with the wind attack angle have a similar trend for the test models of D1, D2 and D3. The maximum values of the aerodynamic lift coefficient for the test models of D1, D2 and D3 appear at the wind attack angle of approximately 90°, which are 0.5, 0.7 and 0.9, respectively. Two local minimum values of the aerodynamic lift coefficients exist for all the test models of D1, D2 and D3 within the wind attack angle regions of 20~40° (around -0.8, -1.0 and -0.35, respectively) and 160~170° (around -0.65, -0.75 and -0.65, respectively). Accordingly, several sudden decrease regions of the aerodynamic lift coefficients for the test models with D-shape ice accretions are identified within the wind attack angle regions of 20~40°, 80~90° and 160~170°. Compared with Fig. 6 of crescent-shape case, it seems that the negative slopes in Fig. 7 of D-shape case are smaller. Unlike the results of the crescent-shape test models, the maximum values of the aerodynamic drag coefficients of the D-shape test models occur at the wind attack angle of 0°.

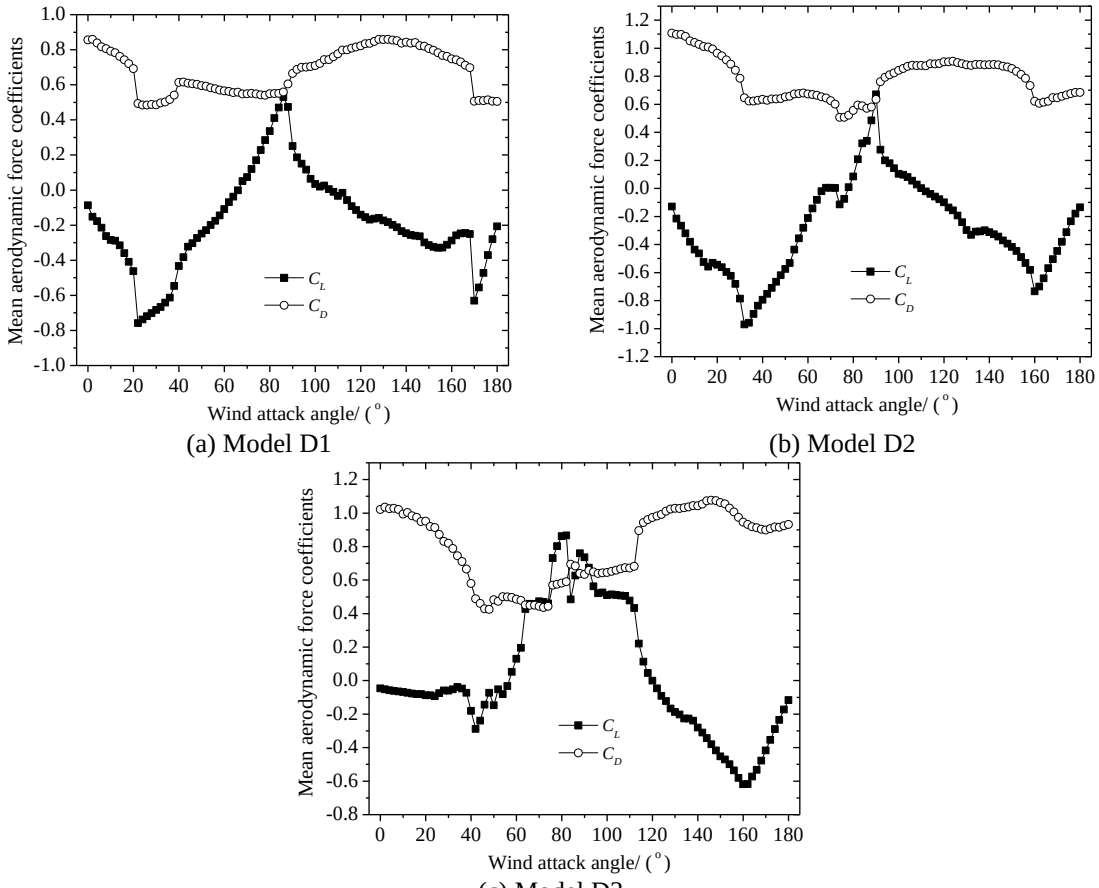


Fig. 7 Aerodynamic drag and lift coefficients for the test models with D-shape ice accretions

### 3.2 Galloping coefficient

According to the classical galloping theory proposed by Den Hartog, the necessary condition for galloping vibration is (Den Hartog 1956)

$$\frac{dC_L}{d\alpha} + C_D < 0 \tag{4}$$

in which, $C_D+dC_L/d\alpha$ is the galloping coefficient.

Figs. 8(a) and 8(b) present the galloping coefficients for the test models with the crescent-shape and D-shape ice accretions, respectively. The local minimum values of galloping coefficients and their corresponding wind attack angles for crescent-shape and D-shape models are summarized in Tables 2 and 3, respectively. It could be found from Fig. 8(a) and Table 2 that the minimum values of galloping coefficients -13.6, -9.7 and -16.9 for the crescent-shape test models C1, C2 and C3, respectively, occur at the wind attack angle of 42°, 180° and 34°, which correspond to the angles associated to the sudden decrease regions of aerodynamic lift coefficient. On the other hand, the minimum values of galloping coefficients -10.4, -10.5 and -10.2 for the D-shape test models D1, D2 and D3, respectively, appear to be larger than those of the crescent-shape test models (except for C2). This indicates that stay cables with crescent-shape ice accretion is more inclined to experience galloping vibration than those with D-shape ice accretion.

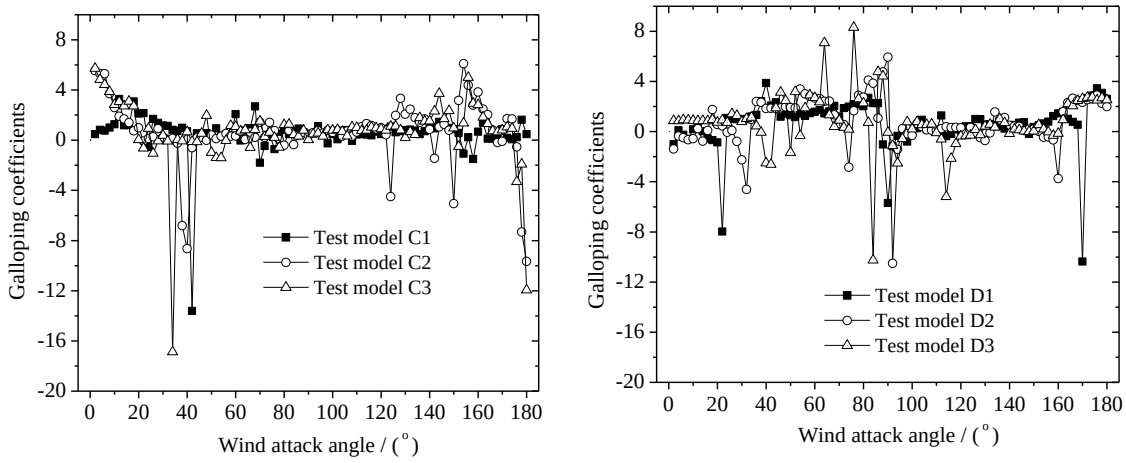


(a) Crescent-shape (b) D-shape

Fig. 8 Galloping coefficients

Table 2 Local minimum values of galloping coefficient for crescent-shape cable

| Test model | C1 | | C2 | | | C3 | |
|---|---|---|---|---|---|---|---|
| Minimum peak value | -13.6 | -8.6 | -4.5 | -5.5 | -9.7 | -16.9 | -11.9 |
| $\alpha$(°) | 42 | 40 | 124 | 150 | 180 | 34 | 180 |

Table 3 Local minimum values of galloping coefficient for D-shape cable

| Test model | D1 | | | D2 | | | D3 | |
|---|---|---|---|---|---|---|---|---|
| Minimum peak value | -8.0 | -5.7 | -10.4 | -4.6 | -10.5 | -3.8 | -2.6 | -10.2 |
| $\alpha$(°) | 22 | 90 | 170 | 32 | 92 | 160 | 42 | 84 |

## 4. Single DOF galloping analysis of iced stay cable

In the aerodynamic instability analysis of iced stay cables in this study, the following assumptions are made: (1) only a particular mode is included; (2) the size and shape of ice accretion are identical along the span of stay cable; (3) the effect of axial flow is neglected; (4) the effect of turbulence in approaching flow is neglected. Based on the above assumptions, a single DOF oscillator of aerodynamics, in which only the vertical vibration is taken into account, can be used to simulate the 3-dimensional continuous stay cable, as indicated in Fig. 9. The aerodynamic forces can be modeled based on the quasi-steady theory with experimentally obtained aerodynamic coefficients. The single DOF oscillator is widely utilized since it could retain the essential aerodynamics of galloping mechanism. Furthermore, due to its simplicity, the single DOF oscillator could facilitate the comprehensive understanding of effects of a series of other factors like mean wind profile and structural properties on the galloping vibration of iced stay cables on the cable-stayed bridges. The equation of motion governing the vertical vibration of the oscillator can be expressed as,

$$m\left(\ddot{y}+2\xi\omega\dot{y}+\omega^2 y\right)=-\frac{1}{2}\rho U^2 B\left[C_D(\alpha+\alpha_r)\sin\alpha_r+C_L(\alpha+\alpha_r)\cos\alpha_r\right] \tag{5}$$

where, $m$ is the mass of the oscillator; $\xi$ is the structural damping ratio; $\omega$ is the circular frequency; $\rho$ is the air density; $U$ is the approaching wind velocity; $B$ is the diameter of the cable; $\alpha$ is the wind attack angle related to the test model; $\alpha_r$ is the variation of wind attack angle due to the vertical vibration of the cable

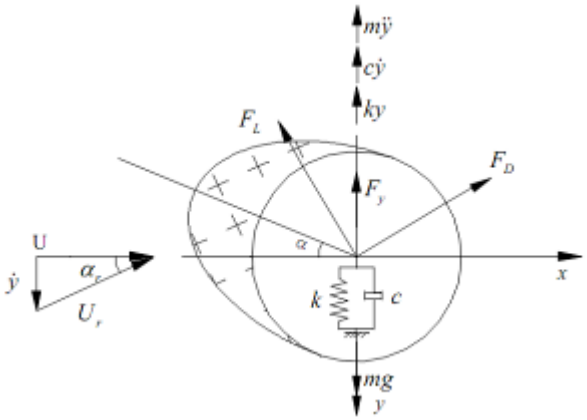


Fig. 9 Single degree-of-freedom model for galloping vibration of iced stay cable

$$\alpha_r = \arctan\frac{\dot{y}}{U} \tag{6}$$

The critical condition of galloping vibration will be satisfied if the sum of structural damping and aerodynamic damping equals to zero, and hence the critical wind velocity of galloping vibration can be obtained from,

$$U_{cr} = -\frac{4m\omega\xi}{\rho B}\cdot\frac{1}{dC_L/d\alpha + C_D} \tag{7}$$

The continuous stay cable in reality is actually an infinite DOF system. Modal analysis is employed in this study to investigate the single-mode galloping mechanism of iced stay cables, where the governing equation of the ith mode of iced stay cable can be written as

$$m_i^*\left(\ddot{y}^* + 2\xi_i\omega_i\dot{y}^* + \omega_i^2 y^*\right) = F_i^*\left(x,t\right) \tag{8}$$

in which

$$m_i^* = \int_0^l \bar{m}\varphi_i^2\left(x\right)dx \tag{9}$$

$$F_i^*\left(x,t\right) = -\int_0^l \frac{1}{2}\rho U^2 B\left[C_D(\alpha+\alpha_r)\sin\alpha_r + C_L(\alpha+\alpha_r)\cos\alpha_r\right]\varphi_i\left(x\right)dx \tag{10}$$

where mi*and Fi*(x,t) are the generalized mass and aerodynamic force of the ith mode of the cable, respectively; y* is the generalized displacement; ωi and ξi are circular frequency and damping ratio of the ith mode of the cable, respectively; φi(x) is the mode shape function of the ith mode of the cable; l is the length of the cable; $\bar{m}$ is the mass of the cable per unit length.

The lowest critical wind velocity of galloping vibration usually corresponds to the fundamental mode of stay cable. Hence, the examination of the critical wind velocity of the fundamental mode is emphasized. The fundamental mode shape φ1(x) could be assumed to be sinπx/l, and hence the corresponding generalized mass and aerodynamic force m1*and F1*(x,t) can be expressed as

$$m_1^* = l\bar{m}/2 \tag{11}$$

$$F_1^*\left(x,t\right) = -\rho U^2 Bl\left[C_D(\alpha+\alpha_r)\sin\alpha_r + C_L(\alpha+\alpha_r)\cos\alpha_r\right]/\pi \tag{12}$$

Substituting Eqs. (11) and (12) into Eq. (8), one obtains,

$$\bar{m}\left(\ddot{y}^* + 2\xi_1\omega_1\dot{y}^* + \omega_1^2 y^*\right) = -\frac{2}{\pi}\rho U^2 B\left[C_D(\alpha+\alpha_r)\sin\alpha_r + C_L(\alpha+\alpha_r)\cos\alpha_r\right] \tag{13}$$

As a result, the corresponding linear critical wind velocity of the fundamental mode of an iced stay cable can be obtained from

$$U_{cr,1} = -\frac{\pi\bar{m}\omega_1\xi_1}{\rho B}\cdot\frac{1}{dC_L/d\alpha + C_D} \tag{14}$$

The critical wind velocity in Eq. (14) corresponds to a particular wind attack angle. It should be

noted that the "effective" wind attack angle, α+αr, depends on the vertical vibration of the oscillator, as shown in Eq. (6). This indicates a nonlinear consideration of the aerodynamic forces of the cable with ice accretion in the calculation of the critical galloping wind velocity at the effective wind attack angle is involved. The nonlinear critical wind velocity could be identified through the relationship between the cable amplitude and wind velocity. In this study, the Runge-Kutta numerical method is adopted to obtain the galloping response of iced stay cable based on Eq. (13) together with the experimental results of the aerodynamic drag and lift coefficients in Sections 2 and 3.

The mean wind profile is not considered in preceding discussions. Let the bridge deck level, zd, as the reference height, mean wind velocity at the height of z, Uz, can be calculated based on the power law and expressed as (Simiu and Scanlan 1996),

$$U_z = U_d \left( z / z_d \right)^{\gamma} \tag{15}$$

$$z = z_d + x \sin \alpha_c \tag{16}$$

where, Ud is the mean wind velocity at the level of bridge deck; αc is the inclined angle of stay cable; x is the distance to the deck end of stay cable; γ is the selected power-law exponent. Substituting Eqs. (15) and (16) into Eq. (10) and let φi(x) = sinπx/l, one has

$$F_i^*(x,t) = -\frac{1}{2}\rho U_d^2 B\left[C_D(\alpha+\alpha_r)\sin\alpha_r + C_L(\alpha+\alpha_r)\cos\alpha_r\right]\times \int_0^l (1+\frac{x\sin\alpha_c}{z_d})^{2\gamma} \sin\frac{\pi x}{l} dx \tag{17}$$

Comparing Eq. (17) with Eq. (12), the relationship between U and Ud can be obtained

$$U_d = U \sqrt{\frac{2l}{\pi \int_0^l (1+\frac{x\sin\alpha_c}{z_d})^{2\gamma} \sin\frac{\pi x}{l} dx}} \tag{18}$$

For a specific stay cable and terrain category, αc, l, zd and γ are known, hence, the relationship between Ud and U could be linearly expressed as

$$U_d = U\beta \tag{19}$$

where β is a constant coefficient for a specific stay cable on the cable-stay bridge. Based on Equation (19), the critical wind velocity, Ucr,1, in uniform flow could be conveniently converted to that in atmospheric boundary flow, Udcr,1.

## 5. Numerical examples

The Yangpu Bridge, which is located in Hainan Province, China, is taken as an example to analyze the galloping responses of stay cable with ice accretion. It is a medium size of cable-stayed bridge with a main span of 460 m, as shown in Fig. 10. The number list of stay cables

from pylon to midspan within the main span is from M1 to M18, and their structural parameters, including the length l, the diameter B, the mass per unit length $\overline{m}$, the fundamental frequency f1, the tensile force Ft and the inclined angle αc, are shown in Table 3. For the longest stay cable M18, l=243.4 m, B=151 mm, f1=0.545 Hz, $\overline{m}$ =96.9 kg/m, Ft=6377 kN, αc=26.9944º. The height of bridge deck zd=50 m, and terrain category "A" is adopted with γ=0.12 according to Chinese Code. The value of β is computed and given in Table 3.

Fig. 10 Elevation view of Yangpu Bridge in Hainan province, China

Table 3 Structural parameters of stay cables of Yangpu Bridge

| Number | $l$ (m) | $\overline{m}$ (kg/m) | $f_1$ (Hz) | $B$ (mm) | $F_t$ (kN) | $\alpha_c$(º) | $\beta$ |
|---|---|---|---|---|---|---|---|
| M1 | 71.3 | 39.7 | 1.87 | 105 | 2599 | 76.90 | 0.940 |
| M2 | 79.0 | 42.2 | 1.69 | 105 | 2726 | 69.20 | 0.937 |
| M3 | 86.5 | 45.7 | 1.54 | 107 | 2969 | 62.54 | 0.936 |
| M4 | 94.6 | 49.2 | 1.31 | 109 | 3135 | 56.87 | 0.934 |
| M5 | 103.2 | 49.2 | 1.30 | 109 | 3260 | 52.05 | 0.933 |
| M6 | 112.5 | 53.2 | 1.19 | 114 | 3542 | 47.99 | 0.931 |
| M7 | 122.2 | 60.8 | 1.06 | 121 | 3793 | 44.58 | 0.930 |
| M8 | 132.3 | 60.8 | 1.00 | 121 | 3909 | 41.64 | 0.929 |
| M9 | 142.7 | 64.5 | 0.92 | 124 | 4118 | 39.14 | 0.928 |
| M10 | 153.3 | 68.6 | 0.85 | 129 | 4356 | 36.99 | 0.927 |
| M11 | 164.1 | 72.6 | 0.80 | 133 | 4622 | 35.12 | 0.925 |
| M12 | 175.1 | 72.6 | 0.76 | 133 | 4774 | 33.47 | 0.924 |
| M13 | 186.3 | 77.7 | 0.70 | 136 | 4989 | 32.06 | 0.923 |
| M14 | 197.5 | 77.7 | 0.68 | 136 | 5228 | 30.77 | 0.922 |
| M15 | 208.9 | 81.7 | 0.64 | 139 | 5453 | 29.66 | 0.921 |
| M16 | 220.3 | 85.9 | 0.61 | 144 | 5702 | 28.67 | 0.919 |
| M17 | 231.8 | 91.3 | 0.58 | 147 | 6176 | 27.77 | 0.918 |
| M18 | 243.4 | 96.9 | 0.55 | 151 | 6377 | 26.99 | 0.917 |

Nonlinear analyses for the galloping responses of iced stay cable utilizing Eqs. (13) and (19) are carried out under selected wind attack angles based on the information given in Tables 1, 2 and 3. Specifically, wind attack angle of 42° for test model C1, 40°, 124°, 150° and 180° for test model C2, 34° and 180° for test model C3, 22°, 90° and 170° for test model D1, 32°, 92° and 160° for test model D2, and 42° and 84° for test model D3 are investigated.

### *5.1 Critical wind velocity*

Nonlinear analyses for galloping responses of all the stay cables listed in Table 3 have been investigated. Fig. 11 presents the critical wind velocity for all stay cables, M1 ~ M18, on the mid-span of the Yangpu Bridge. The structural damping ratio of 1% is adopted, and it is assumed that the ice accretion exists on the full span of the cable. In addition, the ice shape of model C2 and the wind attack angle of 40° are selected for the numerical calculation. It could be found from Fig. 11 that the critical wind velocity of stay cable increases with the decrease of the cable length. Hence, only the results of the longest stay cable M18 under selected wind attack angles with six abovementioned ice shapes are presented here for the sake of brevity. Numerical simulation starts from wind velocity of 1 m/s with an increment of 1 m/s, and stops at 50 m/s, which is higher than the design wind speed (44.7 m/s) at the bridge deck level of the Yangpu Bridge.

The nonlinear critical wind velocities, Ucr,1 and Udcr,1, for crescent-shape and D-shape stay cables under the abovementioned wind attack angles are summarized in Tables 4 and 5, respectively. The minimum nonlinear critical wind velocities at the bridge deck level (Udcr,1) of test models C1, C2, C3, D1, D2 and D3 are 18.3, 18.3, 20.2, 22.0, 27.5 and 27.5 m/s, respectively, corresponding to the wind attack angle of 42°, 40°, 34°, 22°, 92° and 84°. Compared to the design wind speed, the results indicate that galloping vibrations of stay cable M18 may take place if there exist ice accretions.

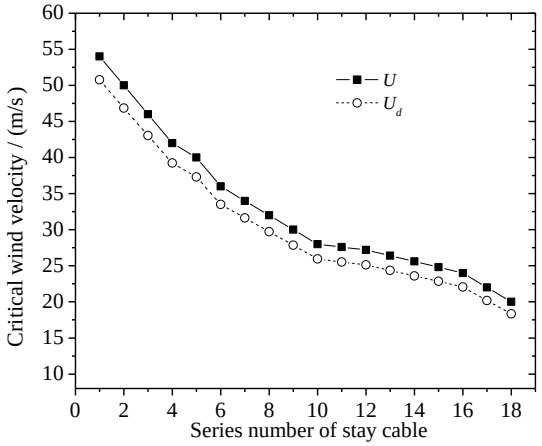


Fig. 11 Critical wind velocities for all stay cables on the mid-span of the Yangpu Bridge (ice shape of model C2, wind attack angle of 40°)

Table 4 Nonlinear critical wind velocities of crescent-shape stay cable

| Test models | C1 | C2 | | | | C3 | |
|---|---|---|---|---|---|---|---|
| Wind attack angles (°) | 42 | 40 | 124 | 150 | 180 | 34 | 180 |
| Critical wind velocity($U_{cr,1}$, m/s) | 20 | 20 | 40 | 28 | 24 | 22 | 28 |
| Critical wind velocity($U_{dcr,1}$, m/s) | 18.3 | 18.3 | 36.7 | 25.7 | 22.0 | 20.2 | 25.7 |

Table 5 Nonlinear critical wind velocities of D-shape stay cable

| Test models | D1 | | | D2 | | | D3 | |
|---|---|---|---|---|---|---|---|---|
| Wind attack angles (°) | 22 | 90 | 170 | 32 | 92 | 160 | 42 | 84 |
| Critical wind velocity($U_{cr,1}$, m/s) | 24 | 52 | 50 | 32 | 30 | 48 | 50 | 30 |
| Critical wind velocity($U_{dcr,1}$, m/s) | 22.0 | 47.7 | 45.9 | 29.3 | 27.5 | 44.0 | 45.9 | 27.5 |

Table 6 Comparison of linear and nonlinear critical wind velocities

| Test models | Wind attack angles (°) | Galloping coefficients | Linear results ($U_{cr,1}$, m/s) | Nonlinear results ($U_{cr,1}$, m/s) |
|---|---|---|---|---|
| C1 | 42 | -13.6 | 2.6 | 20 |
| C2 | 40 | -8.6 | 4.2 | 20 |
| C3 | 34 | -16.9 | 2.1 | 22 |
| D1 | 22 | -8.0 | 4.5 | 24 |
| D2 | 92 | -10.5 | 3.4 | 30 |
| D3 | 84 | -10.2 | 3.5 | 30 |

The linear critical wind velocity could be obtained from Eq. (14) by utilizing the local minimum values of galloping coefficients shown in Tables 1 and 2. These results are listed in Table 6 (Column 4), together with those obtained from nonlinear analyses (Column 5). It is found that the obtained linear critical wind velocity (within the range from 2.1 to 4.5 m/s) is far smaller than the nonlinear value (within the range from 20 to 30 m/s). Hence, the critical galloping wind velocity will be underestimated by using the local minimum values of galloping coefficient. This is mainly due to the relative large contribution from the vertical vibration of cable to the "effective" wind attach angle.

Fig. 12 presents the cable amplitudes (one-side) at various wind velocities (Uniform flow, U) for ice accretions of C1, C2, C3, D1, D2 and D3, respectively. It could be found from Fig. 12 that the increase of cable amplitude with the wind velocity beyond the critical value is relatively not very intensive. This may result from the extremely narrow range of the negative slope of the

aerodynamic lift coefficient of the iced stay cables, as presented in Figs. 6 and 7. In this case, the "effective" wind attack angle is very easy to move out of the negative slope range (Wu *et al*. 2013).

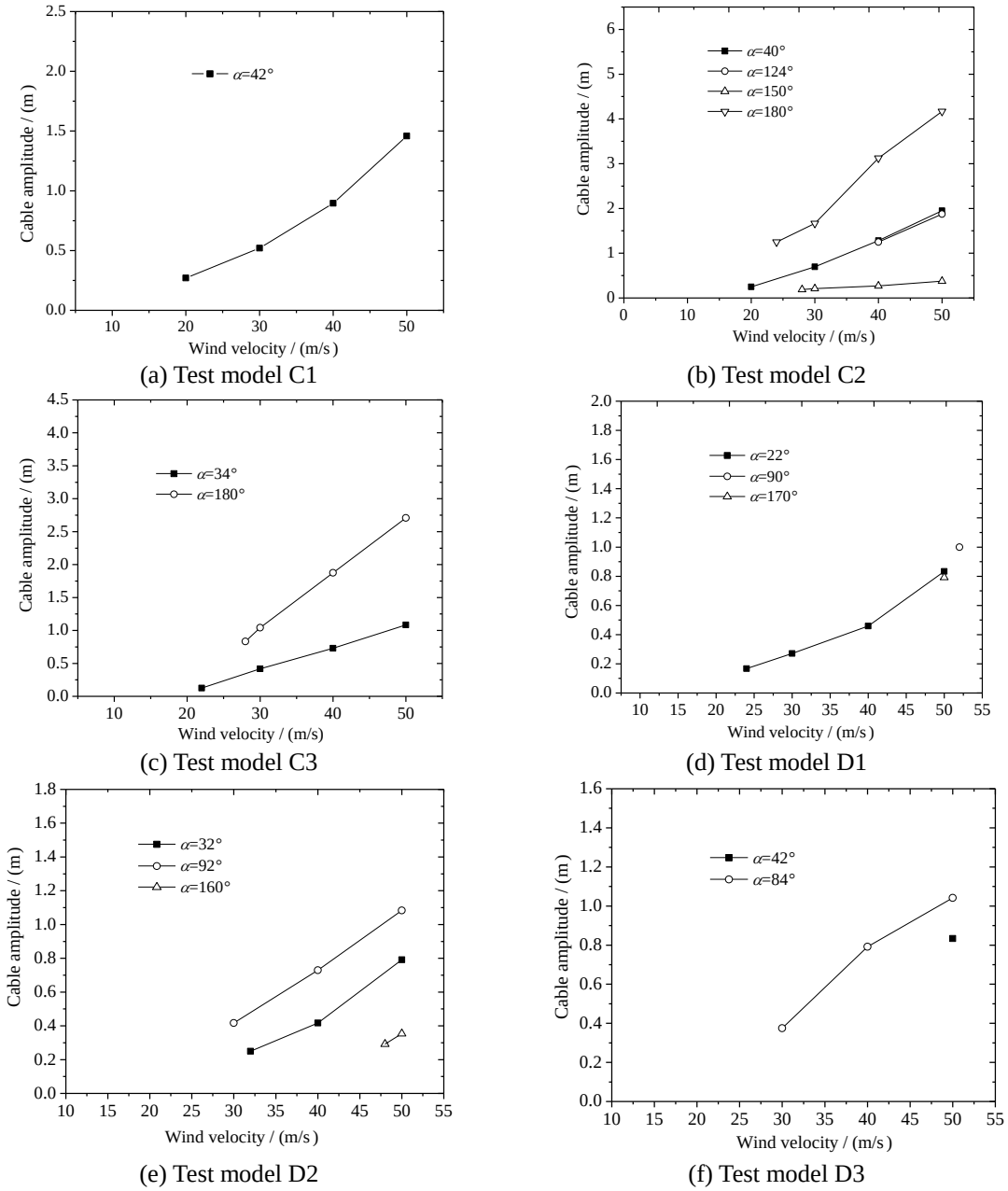


(a) Test model C1 (b) Test model C2

(c) Test model C3 (d) Test model D1

(e) Test model D2 (f) Test model D3

Fig. 12 Cable amplitudes of M18 at selected wind velocity for various ice accretions

For example, the one-side amplitude for test model C2 at the wind velocity of 20 m/s with an wind attack angle of 40° is about 0.24 m, which contributes an "effective" wind attack angle of 4.71° to the galloping system. This value is larger than the region of sudden decrease of the aerodynamic lift coefficient, approximately 2° as indicated in Fig. 6. This situation becomes even more obvious for high modes of the stay cables (with higher oscillation frequency). Assuming the cable vibrate harmonically, the amplitude of velocity of the cable, which contributes to the "effective" wind attack angle as indicated in Eq. (6) will be the amplitude of displacement multiplied by the vibrating frequency.

Figs. 13(a)-13(f) present time histories of the displacement of the cable under the wind velocities U=15, 19, 20, 30, 40, 50 m/s for the test models C2, respectively. Wind attack angle is selected to be 40°, which is the most susceptible to galloping vibration. Obviously, the cable vibration will be convergent if the wind velocity is smaller than the critical wind velocity, as shown in Figs. 13(a) and 13(b). Also, if the wind attack angle is not fixed within the sudden decrease region of the aerodynamic lift coefficient, the cable is stable even if the wind velocity is up to 50 m/s, as given in Fig. 13(g).

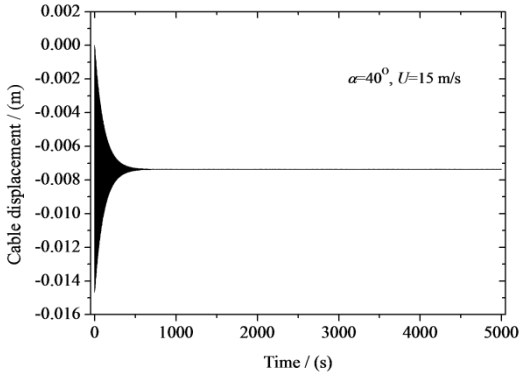


(a) α=40º, U=15 m/s

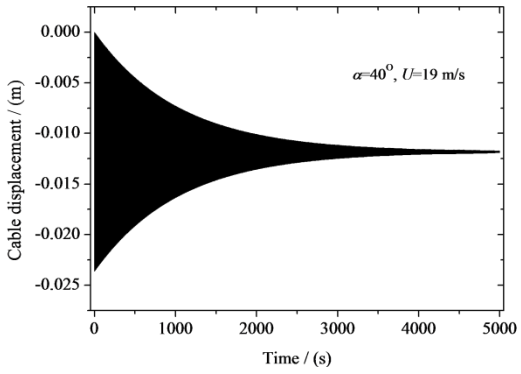


(b) α=40º, U=19 m/s

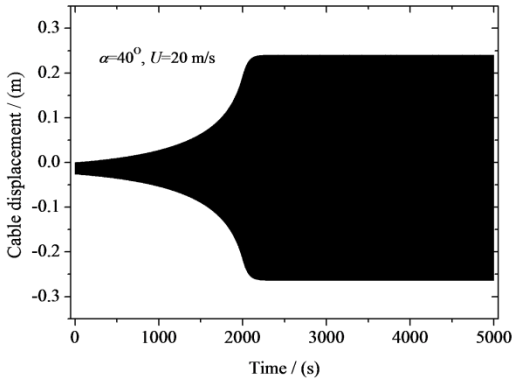


(c) α=40º, U=20 m/s

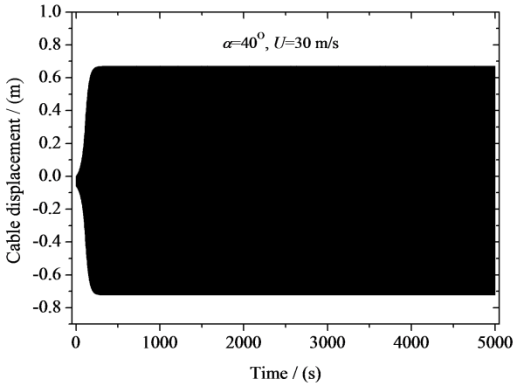


(d) α=40º, U=30 m/s

Continued-

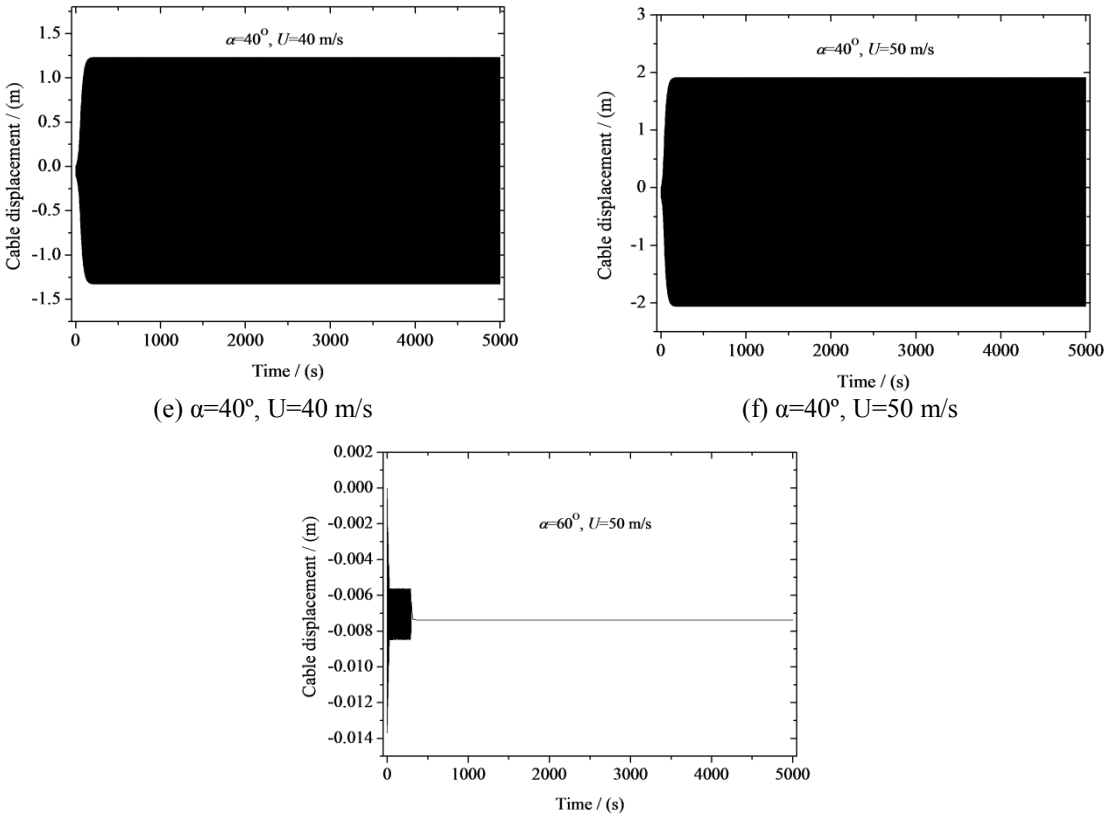


(e) α=40º, U=40 m/s (f) α=40º, U=50 m/s

(g) α=60°, U=50 m/s

Fig. 13 Time histories of the displacement of cable vibration (test model C2)

### *5.2 Effects of longitudinal distribution of ice accretion along the cable*

Although the galloping critical wind velocity of the stay cable M18 of the Yangpu Bridge is lower than the design wind velocity, it is a rare event that all the above mentioned conditions for galloping vibration are concurrently satisfied. For example, the ice accretion may be coagulated only on a part of the stay cable, rather than the full span. Fig. 14 presents the nonlinear critical galloping wind velocity at the bridge deck level of the stay cable M18 for different lengths of ice accretion (ice shape of model C2) formed on the cable. The wind attack angle of 40° is adopted. Four types of the distribution of ice accretion, l/4, l/2, 3l/4 and l, are considered, where the ice accretion always starts from the cable end at the pylon. It could be found from Fig. 14 that the critical wind velocity increases with the decrease of the length of the ice accretion. The critical wind velocities at the bridge deck level are 18.3, 22.0, 42.2 and 124.7 m/s for the length of ice accretion of l, 3l/4, l/2 and l/4, respectively. It should be noted that, even if the ice accretion exists along the full span of the cable, the shape may change at various locations.

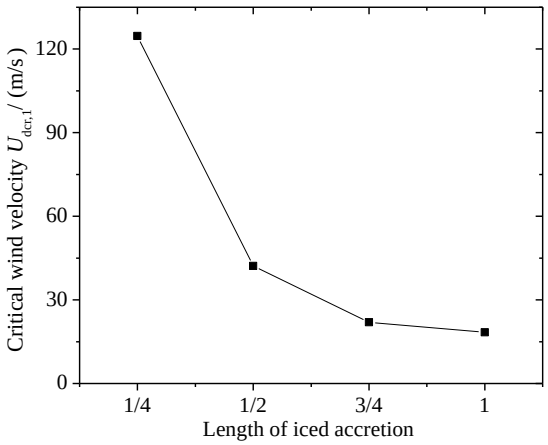


Fig. 14 Nonlinear critical galloping wind velocities with the ice accretion length

### 5.3 Effects of structural damping

One widely-used countermeasure to mitigate the wind-induced vibration of stay cable is to increase effective structural damping, e.g., by installing dampers near the end of the cable. Fig. 15 presents the relationship between the nonlinear critical galloping wind velocity and the structural damping ratio for the stay cable M18, where the structural damping ratios of 0.1%, 0.2%, 0.5%, 1%, 2% and 5% are examined. The ice shape of model C2 and the wind attack angle of 40° are adopted here. It could be found from Fig. 15 that the critical wind velocity of stay cable decreases linearly with the increase of the structural damping ratio. The critical wind velocity is as low as 5.5 m/s for the structural damping ratio of 0.1%, while the critical wind velocity can be enhanced to 78.9 m/s, which is higher than the design wind velocity at the bridge deck level, 44.7 m/s, for the structural damping ratio of 5%. Consequently, it appears that increasing structural damping is an effective approach for the mitigation of galloping vibration of stay cable with ice accretion.

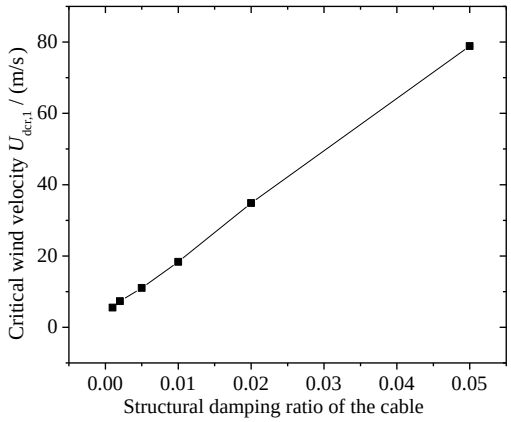


Fig. 15 Nonlinear critical galloping wind velocities with structural damping ratio

## 6. Conclusions

The galloping vibration of stay cables with ice accretions on a medium-span cable-stayed bridge is comprehensively investigated. Six iced cable models, including three types of crescent-shape (C1, C2 and C3) and three types of D-shape (D1, D2 and D3), are tested in the wind tunnel with a geometric scale of 1:1 to identify their aerodynamic drag and lift coefficients. Sudden decreases of the aerodynamic lift coefficients are observed for all six test models. The galloping coefficients, which are widely applied to the classical galloping theory and calculated based on the measured aerodynamic force coefficients, have the minimum values of -13.6, -9.7, -16.9, -10.4, -10.5 and -10.2 for test models of C1, C2, C3, D1, D2 and D3, respectively. Both linear and nonlinear critical galloping wind velocities are analyzed utilizing a single degree-of-freedom model based on the quasi-steady theory together with the experimentally identified aerodynamic force coefficients. The nonlinear results show that the minimum critical wind velocities for the longest stay cable of the Yangpu Bridge are respectively 18.3, 18.3, 20.2, 22.0, 27.5 and 27.5 m/s corresponding to test models C1, C2, C3, D1, D2 and D3. Typically, the linear critical galloping wind velocities are far lower than those from nonlinear analyses. It should be noted that these nonlinear critical galloping wind velocities are lower than the design wind velocity at the bridge site. On the other hand, there exist limit cycle oscillations of the iced stay cables beyond the nonlinear critical galloping wind velocity. The main reason is that the sudden decrease region of the mean lift coefficient is so narrow that the cable can easily move out of it even for small oscillation amplitude of stay cables. In addition, the effects of longitudinal distribution of ice accretion and structural damping on the nonlinear critical galloping wind velocity are investigated. The results demonstrate that a shorter ice accretion and a larger structural damping will both result in a larger critical wind velocity.

Several issues should be considered before a conclusion for the possible galloping vibration of stay cable with ice accretion is given. Usually, the extreme wind speed and the serious ice disaster may not be likely to occur simultaneously. Also, the critical wind velocity might be higher than the results of this study considering the effects of the variation of the size and shape of ice accretion along the cable and the oncoming turbulence.

## Acknowledgements

This project was jointly supported by the National Basic Research Program of China (973 Program: 2015CB057702), the National Natural Science Foundation of China (51578234), National Science Foundation (CMMI 15-37431) to which the authors gratefully appreciate.

## References

Alto, P. (1979), EPRI Transmission Line Reference Book: Wind-Induced Conductor Motion, Electric Power Research Institute, California, USA.

Cheng, S.H., Larose, G.L., Savage, M.G., Tanaka, H. and Irwin, P.A. (2008a), "Experimental study on the wind-induced vibration of a dry inclined cable-Part I: Phenomena", *J. Wind Eng. Ind. Aerod.*, **96**(12), 2231-2253.

Cheng, S.H., Irwin, P.A. and Tanaka, H. (2008b), "Experimental study on the wind-induced vibration of a dry inclined cable-Part II: Proposed mechanisms", *J. Wind Eng. Ind. Aerod.*, **96**(12), 2254-2272.

Demartino, C., Koss, H.H., Georgakis, C.T. and Ricciardelli, F. (2015), "Effects of ice accretion on the aerodynamics of bridge cables", *J. Wind Eng. Ind. Aerod.*, **138**, 98-119.
Demartino, C. and Ricciardelli, F. (2015), "Aerodynamic stability of ice-accreted bridge cables", *J. Fluid. Struct.*, **52**, 81-100.
Den Hartog, J.P. (1956), "Mechanical Vibrations", New York: McGraw-Hill.
Farzaneh, M. (2008), Atmospheric icing of power networks, Springer, New York.
Flamand, O. and Boujard, O. (2009), "A comparison between dry cylinder galloping and rain-wind induced vibration", *Proceedings of the EACWE5*, Florence, Italy.
Fu, P., Farzaneh, M. and Bouchard, G. (2006), "Two-dimensional modeling of the ice accretion process on transmission line wires and conductors", *Cold Regions Sci. Technol.*, **46**(2), 132-146.
Gimsing, N.J. and Georgakis, C.T. (2012), Cable supported bridge: Concept and design, Wiley, Chichester, England.
Gjelstrup, H. and Georgakis, C.T. (2011), "A quasi-steady 3 degree-of-freedom model for the determination of the onset of bluff body galloping instability", *J. Fluid. Struct.*, **27**(7), 1021-1034.
Gjelstrup, H., Georgakis, C.T. and Larsen, A. (2012), "An evaluation of iced bridge hanger vibrations through wind tunnel testsing and quasi-steady theory", *Wind Struct.*, **15**(5), 385-407.
Hikami, Y. and Shiraishi, N. (1988), "Rain-wind induced vibrations of cables in cable stayed bridges", *J. Wind Eng. Ind. Aerod.*, **29**, 409-418.
Jones, N.P., Jain, A. and Pan, K. (1997), "Effect of stay cable vibration on buffeting response", *Proceedings of the Structures Congress '97 ASCE*, Portland.
Kollár, L.E. and Farzaneh, M. (2010), "Wind-tunnel investigation of icing of an inclined cylinder", *Int. J. Heat Mass Tran.*, **53**(5-6), 849-861.
Koss, H.H., Henningsen, J.F. and Olsen, I. (2013), "Influence of icing on bridge cable aerodynamics", *Proceedings of the 15th International Workshop on Atmospheric Icing of Structures (IWAIS XV)*, Session 6.
Koss, H.H., Gjelstrup, H. and Georgakis, C.T. (2012), "Experimental study of ice accretion on ciicular cylinders at moderate low temperatures", *J. Wind Eng. Ind. Aerod.*, **104-106**, 540-546.
Latforte, J.L., Phan, L.C. and Du, N.D. (1984), "Preliminary investigation on effect of wind speed fluctuations on ice accretions grown on fixed and rotating aluminium conductor", *Proceedings of the 2nd Int. Workshop on Atmospheric Icing of Structures*, Trondheim, Norway.
Li, S.Y., Chen, Z.Q., Dong, G.C. and Luo, J.H. (2014), "Aerodynamic stability of stay cables incorporated with lamps: a case study", *Wind Struct.*, **18**(1), 83-101.
Li, S.Y., Chen, Z.Q., Teng, W. and Kareem, A. (2013), "Rain-wind induced in-plane and out-of-plane vibrations of stay cables", *J. Eng. Mech. - ASCE*, **139**(12), 1688-1698.
Lu, M.L., Popplewell, N. and Shah, A.H. (2000), "Freezing rain simulations for fixed, unheated conductor samples", *J. Appl. Meteorol.*, **39**(12), 2385-2396.
Macdonald, J.H.G. and Larose, G.L. (2006), "A unified approach to aerodynamic damping and drag/lift instabilities, and its application to dry inclined cable galloping", *J. Fluid. Struct.*, **22**(2), 229-252.
Macdonald, J.H.G. and Larose, G.L. (2008a), "Two-degree-of-freedom inclined cable galloping – Part 1: General formulation and solution for perfectly tuned system", *J. Wind Eng. Ind. Aerod.*, **96**(3), 291-307.
Macdonald, J.H.G. and Larose, G.L. (2008b), "Two-degree-of-freedom inclined cable galloping – Part 2: Analysis and prevention for arbitrary frequency ratio", *J. Wind Eng. Ind. Aerod.*, **96**(3), 308-326.
Matsumoto M., Yagi, T., Shigemura, Y. and Tsushima, D. (2001), "Vortex-induced cable vibration of cable-stayed bridges at high reduced wind velocity", *J. Wind Eng. Ind. Aerod.*, **89**(7-8), 633-647.
Matsumoto, M., Yagi, T., Hatsuda, H., Shima, T., Tanaka, M. and Naito, H. (2010), "Dry galloping characteristics and its mechanism of inclined/yawed cables", *J. Wind Eng. Ind. Aerod.*, **98**(6-7), 317-327.
Novak, M. and Tanaka, H. (1974), "Effect of turbulence on galloping instability", *J. Eng. Mech. - ASCE*, **100**(1), 27-47.
Parkinson, G.V. and Smith, J.D. (1964), "The square prism as an aeroelastic non-linear oscillator", *Q. J. Mech. Appl. Math.*, **17**, 225-239.
Poots, G. (1996), Ice and snow accretion on structures, Research Studies Press Ltd., Somerset, UK.
Simiu, E. and Scanlan, R.H. (1996), Wind effects on structures, Wiley, New York.

Stumpf, P. (1994), "Determination of aerodynamic forces for iced single and twin-bundled conductors", M. Sc. Thesis, Department of Mechanical and Industrial Engineering, University of Manitoba.
Wu, T., Kareem, A. and Li, S. (2013), "On the excitation mechanisms of rain-wind induced vibration of cables: Unsteady and hysteretic nonlinear features", *J. Wind Eng. Ind. Aerod.*, **122**, 83-95.
Yu, P., Desai, Y.M., Shah, A.H. and Popplewell, N. (1993a), "Three-degree-of-freedom model for galloping, Part I: Formulation", *J. Eng. Mech. - ASCE*, **119**(12), 2404-2425.
Yu, P., Desai, Y.M., Popplewell, N. and Shah, A.H. (1993b), "Three-degree-of-freedom model for galloping, Part II: Solutions", *J. Eng. Mech. - ASCE*, **119**(12), 2426-2448.
Zuo, D., Jones, N.P. and Main, J.A. (2008), "Field observation of vortex- and rain-wind-induced stay-cable vibrations in a three-dimensional environment", *J. Wind Eng. Ind. Aerod.*, **96**(6-7), 1124-1133.

*CC*